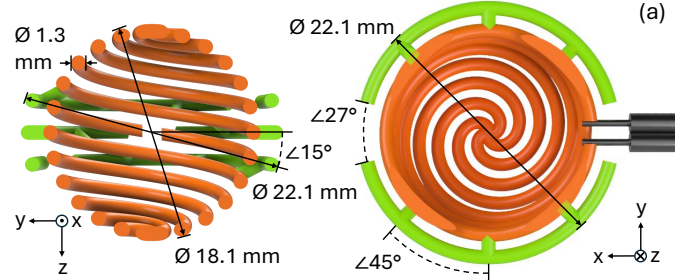


# An Electrically Small Circularly Polarized Spherical Folded Helix Antenna for GPS

Edward Wawrzynek, Songyi Yen, Ljubodrag Boskovic, and Dejan Filipovic

University of Colorado Boulder, CO, USA {edward.wawrzynek,songyi.yen,ljubodrag.boskovic,dejan}@colorado.edu

**Abstract**—The design and experimental verification of an electrically small modified spherical folded helix antenna are reported. The antenna generates circular polarization from aligned electric and magnetic dipoles excited by a single port. Through the design of parasitic loop elements, the axial ratio of the antenna is reduced to below 3 dB over most of the field-of-view. A prototype antenna is monolithically fabricated through stereolithography and achieves good agreement with simulation. The antenna is self-resonant at an electrical size of  $ka = 0.29$  and achieves instantaneous coverage of the GPS L5 band.



## I. INTRODUCTION

Electrically small antennas have benefits for space constrained applications at the cost of fundamental bandwidth limitations [1]. For narrowband use, such as the global positioning system (GPS), electrically small antennas offer the possibility of high efficiency and a compact spatial profile. In this application, circular polarization is desirable for the reduction of both multipath effects and polarization mismatch [2]. Further, a broad radiation pattern is useful to achieve coverage of a large portion of the sky.

The spherical folded helix, formed from wires coiled into a helix about the surface of a sphere, can be designed to have a resonance in the electrically small region with a quality factor near the fundamental limit [3]. Constructed as a linearly polarized monopole over a ground plane, the helix has been experimentally verified through various fabrication methods [4]–[6], including usage as a sensing platform for GPS signals [6].

The helix can be constructed as a circularly polarized dipole, a design which has been investigated numerically [3], [7], [8]. To the authors’ knowledge, there are no reported experimental verifications of the spherical folded helix as a circularly polarized antenna.

This work proposes a spherical helix antenna modified for usage as a GPS antenna over the L5 band at 1.1702 to 1.1827 GHz. The proposed antenna and fabricated prototype are shown in Fig. 1. The design incorporates parasitic loop elements which both lower the antenna’s axial ratio and excite evanescent spherical modes which can be used to adjust the helix’s resonance.

## II. HELIX DESIGN

The design evolution begins with the spherical folded helix described in [3], an example of which is shown in Fig. 2a. The helix is parameterized by its number of arms and how tightly each arms is wound on the sphere. To remain consistent with [3], the number of turns per arm is defined as the number

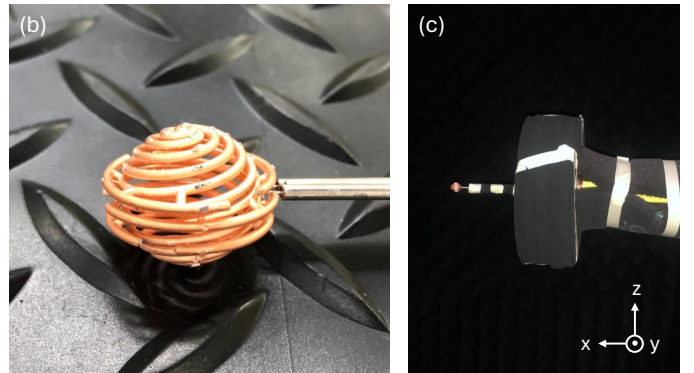


Fig. 1: Split view of the proposed antenna, showing (a) the folded spherical helix model, (b) a fabricated prototype, and (c) measurement setup.

of revolutions made by an arm about the  $z$  axis in a single hemisphere of the helix.

The properties of the helix are numerically investigated in Altair FEKO and Ansys HFSS. The miniaturization properties of the helix are plotted in Fig. 3. The resonant frequency of the helix, inversely proportional to the electrical size  $ka$ , is mainly determined by the number of turns of each arm. More turns contribute to increased miniaturization and a corresponding increase in the quality factor  $Q$  of the antenna. Increasing the number of arms in the helix has little effect on the electrical size but leads to a decrease in  $Q$ .

The currents on the helix are in-phase, exciting aligned electric ( $TM_{10}$ ) and magnetic ( $TE_{10}$ ) dipole modes. Except at the poles ( $\theta = 0^\circ, 180^\circ$ ) of the helix, radiation is dominated by these two dipole modes. Because they are excited in phase, there is an orthogonal phase relationship between their respective far fields [9], giving the helix elliptically polarized radiation. The amplitude ratio of  $TM_{10}$  and  $TE_{10}$  is therefore equivalent to the antenna’s axial ratio where radiation is significant. This amplitude ratio is plotted in Fig. 4 as a function of the helix design parameters. With no turns per



Fig. 2: Design evolution of the proposed antenna, showing (a) the base 4 arm, 1.5 turn folded spherical folded helix, (b) addition of a parasitic loop around the antenna to reduce axial ratio, (c) multiple parasitic loops, and (d) the introduction of cuts in the parasitic loops for tuning of the resonant frequency.

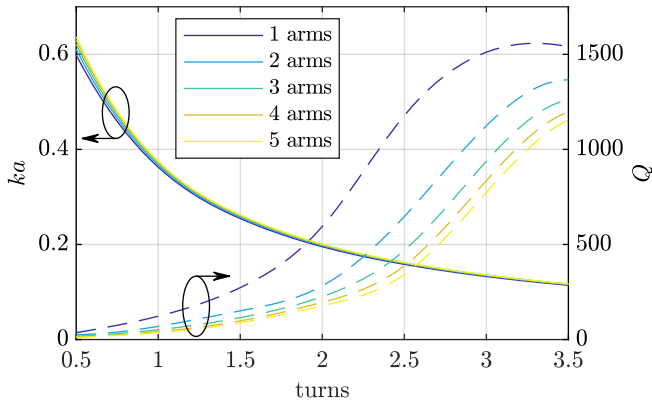


Fig. 3: The resonant electrical size  $ka$  and quality factor  $Q$  of the spherical helix as a function of the number of arms in the helix and turns per arm.

arm, the helix is a multi-arm folded dipole and the radiated fields are dominated by  $TM_{10}$ . As the number of turns is increased, the helix increasingly couples into  $TE_{10}$ , with the ratio between the two modes settling towards 3 dB.

The helix is resonant when the reactive stored energy is zero, that is, when the  $TM_{10}$  and  $TE_{10}$  modes have equal contributions to the stored energy. At small electrical size, the  $TM_{10}$  mode radiates more power relative to its stored energy than the  $TE_{10}$  mode. Thus, when the helix is in resonance, the modes in far field are imbalanced, resulting in an elevated axial ratio.

The radiation resistance of the helix is plotted in Fig. 5 as a function of design parameters. It is possible to achieve a  $50 \Omega$  impedance without a tuning network over a wide range of  $ka$  through an appropriate choice of the number of arms.

#### A. Parasitic Loop Design

The currents which exist on the helix are a superposition of those exciting a pure  $TM_{10}$  mode and  $TE_{10}$  mode [10],

$$\mathbf{J}_{TM_{10}} = J_{TM_{10}} \sin(\theta) \hat{\theta}, \quad (1)$$

$$\mathbf{J}_{TE_{10}} = J_{TE_{10}} \sin(\theta) \hat{\phi}, \quad (2)$$

where  $J_{TM_{10}}$  and  $J_{TE_{10}}$  are the amplitudes of current density for the respective modes.

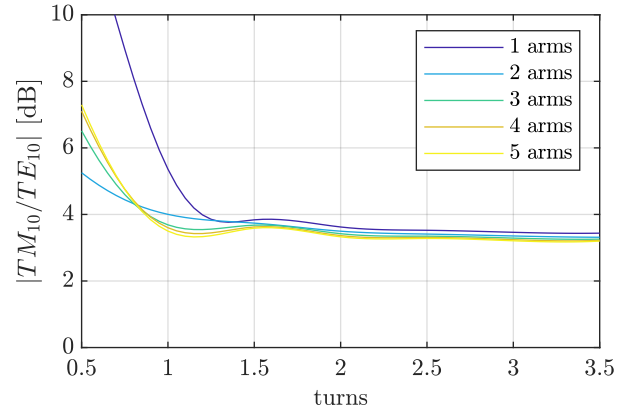


Fig. 4: The amplitude ratio of the  $TM_{10}$  and  $TE_{10}$  modes radiated by the helix as a function of the number of arms and turns per arm.

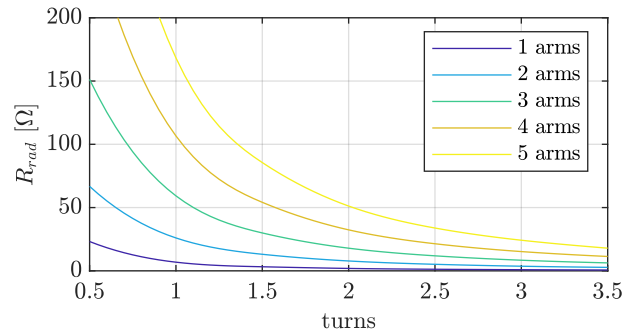


Fig. 5: Radiation resistance of the spherical helix at resonance as a function of the number of arms and turns per arm.

The helix shown in Fig. 2a has an axial ratio of 3.6 dB. Reduction of the helix's axial ratio requires increased coupling in  $TE_{10}$  relative to  $TM_{10}$ . To do so, conductive loops aligned with the currents in (2) are placed around the outside of the helix. The effects of both 1 and 3 loops around the antenna are considered, shown in Fig. 2b and 2c, respectively. These loops are effective at reducing the axial ratio of the helix to 2.6 dB and 1.5 dB, respectively. However, due to the stored energy added by the loops, they increase the resonant frequency by a factor of 1.3 and 1.6, respectively.

To reduce the resonant frequency, the energy contributed

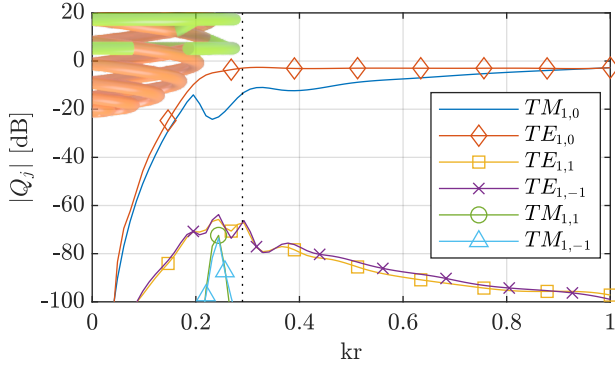


Fig. 6: Spherical mode decomposition of the near field around the proposed antenna. The antenna model inset in top left is aligned with the  $kr$  axis.

by the  $TE_{10}$  mode must be compensated. By placing cuts in the loops around the helix, shown in Fig. 2d, extra capacitive energy is introduced into the near field, restoring the resonant frequency of the helix to the L5 band. In the near field, this extra energy exists within higher order spherical modes. Due to the antenna's small electrical size, these modes cannot be efficiently radiated [10]. The near field modal decomposition of the antenna is shown in Fig. 6, using the outward propagating spherical modes defined in [10]. Higher order modes are present near the loops, but their amplitude decays moving into the far field, while the  $TM_{10}$  and  $TE_{10}$  modes radiate into the far field. The cuts reduce the loops' effectiveness at coupling into  $TE_{10}$ , raising the axial ratio to 2.5 dB.

### B. Prototype Antenna

The final design is shown in Fig. 1a. The antenna is a four arm helix with 1.5 turns per arm, with a helix diameter of 18mm and loops of diameter 22mm around the helix. The cuts placed in the loops are  $27^\circ$  wide, establishing resonance at the center of the L5 band. To enable simple fabrication, radially oriented supports are placed between the inner arms of the helix and the parasitic loops. Because the radial fields of the antenna are weak in this region, the currents excited on these supports are small and have little impact on the antenna's electrical characteristics.

The antenna is fabricated through stereolithographic 3D printing followed by copper electroplating. The integration of the parasitic loops to be electrically connected to the inner helix allows for simple monolithic fabrication of the entire structure.

The fabricated prototype is excited by a feedline oriented in the equatorial plane of the antenna, where radial near fields are weak. For measurement purposes, the feed is composed of a balanced bundle of two coaxial cables. The antenna's  $50 \Omega$  match could lend itself to the integration of a balun in the feeding region.

Because the  $TE_{10}$  and  $TM_{10}$  modes have no phase variation over the sphere, they have a stable phase center as seen from any angle. The phase variation of the high order modes excited in the near field has little effect in the far field, leading

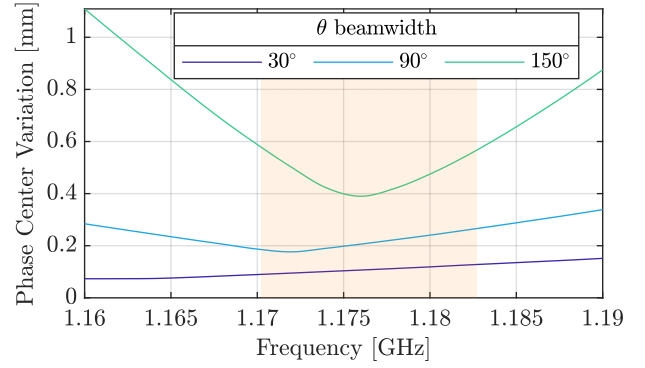


Fig. 7: Simulated phase center stability of the proposed antenna. Phase center variation is taken over all  $\phi$  angles and variable beamwidth in  $\theta$ , centered about  $\theta = 90^\circ$ . The GPS L5 band is highlighted.

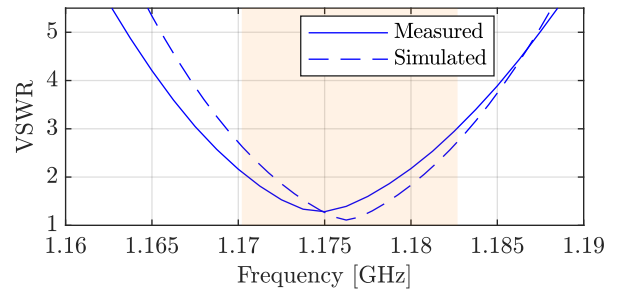


Fig. 8: Measured and simulated VSWR of the prototype antenna. The GPS L5 band is highlighted.

to a stable overall phase center, plotted in Fig. 7. Over a  $150^\circ$  beamwidth in  $\theta$ , the maximum simulated phase center variation is less than 0.6mm, or  $\lambda/420$ .

## III. RESULTS

The simulated and measured impedances of the antenna are shown in Fig. 8. The antenna is resonant at 1.175 GHz with an electrical size of  $ka = 0.29$ . The antenna covers the entire L5 band at VSWR less than 3:1, and achieves a VSWR 2:1 bandwidth of 8.7 MHz. The antenna's measured quality factor, derived as described in [11], is 2.05 times the limit given in [1]. That  $Q$  is elevated beyond the minimum limit is in part a consequence of the higher order modes excited in the near field, a trade-off between axial ratio and bandwidth which is analytically quantified in [9].

The measured radiation patterns of the antenna are shown in Fig. 9. The presence of absorber placed near the antenna in the measurement setup, shown in Fig. 1c, causes significant scattering, leading to pattern asymmetry and elevated cross-polarization. This is reflected in the variation of the pattern between the cuts plotted. Simulation of the measurement setup gives patterns which display most of the features seen in measurement.

To understand the free space characteristic of the antenna, the measured patterns are processed through the mathematical absorber reflection suppression (MARS) as described in [12].

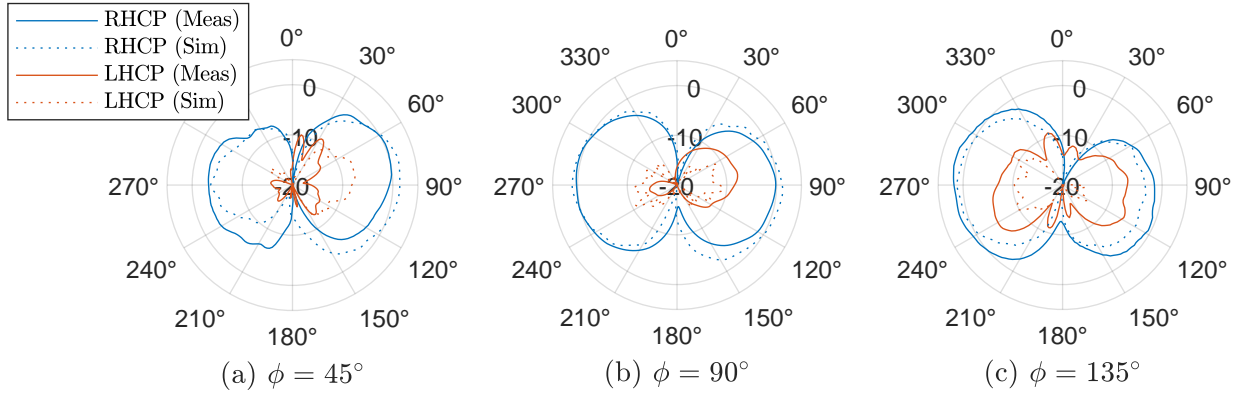


Fig. 9: Measured and simulated directivity patterns of the prototype antenna. Patterns are taken at the antenna’s resonance, 1.175GHz.

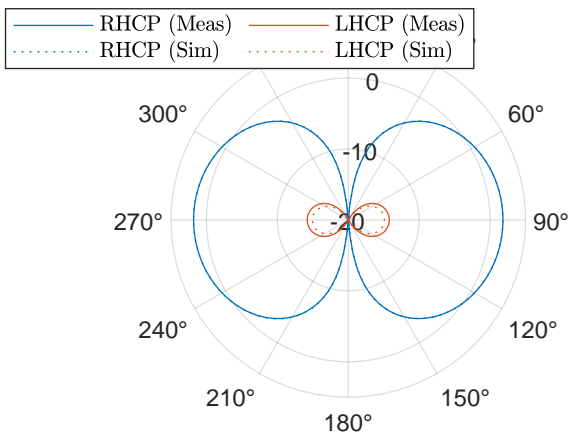


Fig. 10: Free space simulated and measured directivity patterns of the prototype antenna after scattering suppression.

Given the small size of the antenna, radiation observed in high order spherical modes is suspected to originate from a scatterer in the measurement setup larger than the antenna itself. Truncation of modes in the measurement to  $TM_{10}$  and  $TE_{10}$  only therefore reduces the effects of scatterers in the setup.

The directivity of the antenna after application of MARS is shown in Fig. 10. At the equator, the pattern has a cross polarization discrimination of 16.2dB, corresponding to an axial ratio of 2.7dB. The measured  $TM_{10}$  and  $TE_{10}$  modes have an amplitude ratio of 2.6dB and are  $5^\circ$  out of phase, suggesting that the modal excitation of the prototype antenna matches well with that of the design.

#### IV. CONCLUSION

A modified spherical folded helix antenna is designed for resonance in the GPS L5 band, achieving an electrical size of  $ka = 0.29$ . Parasitic loop elements integrated into the antenna allow for control of the antenna’s coupling into the electric and magnetic dipole modes, giving the antenna an axial ratio below 3dB across most of the field-of-view. The

antenna displays a dipole radiation pattern and stable phase center across the band of interest. A fabricated prototype of the antenna agrees well with simulated results and validates the successful modification of the helix’s modal content.

#### ACKNOWLEDGEMENT

This work is funded by the Office of Naval Research under the grant N00014-23-1-2120.

#### REFERENCES

- [1] R. Collin and S. Rothschild, "Evaluation of antenna Q," in *IEEE Trans. Antennas Propag.*, vol. 12, no. 1, pp. 23-27, January 1964.
- [2] J. I. Ortigosa, N. Padros and M. F. Iskander, "Comparative study of high performance GPS receiving antenna designs," *IEEE Antennas and Propagation Society International Symposium 1996 Digest*, Baltimore, MD, USA, 1996, pp. 1958-1961.
- [3] S. R. Best, "Low Q electrically small linear and elliptical polarized spherical dipole antennas," in *IEEE Trans. Antennas Propag.*, vol. 53, no. 3, pp. 1047–1053, March 2005.
- [4] J. J. Adams, S. C. Slimmer, T. F. Malkowski, E. B. Duoss, J. A. Lewis and J. T. Bernhard, "Comparison of Spherical Antennas Fabricated via Conformal Printing: Helix, Meanderline, and Hybrid Designs," in *IEEE Antennas Wireless Propag. Lett.*, vol. 10, pp. 1425-1428, 2011.
- [5] O. S. Kim, "Rapid Prototyping of Electrically Small Spherical Wire Antennas," in *IEEE Trans. Antennas Propag.*, vol. 62, no. 7, pp. 3839-3842, July 2014.
- [6] C. Y. Kataria, G. X. Gao and J. T. Bernhard, "Design of a Compact Hemispherical GPS Antenna With Direction Finding Capabilities," in *IEEE Trans. Antennas Propag.*, vol. 67, no. 5, pp. 2878-2885, May 2019.
- [7] O. S. Kim, "Minimum Q Electrically Small Antennas," in *IEEE Trans. Antennas Propag.*, vol. 60, no. 8, pp. 3551-3558, Aug. 2012.
- [8] E. Wawrzyniec, S. Yen, and D. Filipovic, "Design of an Electrically Small Circularly Polarized Spherical Folded Helix Antenna", *2025 United States National Committee of URSI National Radio Science Meeting (USNC-URSI NRSM)*, Boulder, CO, USA 2025.
- [9] A. B. Murray and A. K. Iyer, "Analytical expressions for spherical wire antenna quality factor demonstrating exact agreement between circuit-based and field integration techniques," in *IEEE Trans. Antennas Propag.*, vol. 72, no. 2, pp. 1636–1647, Feb. 2024.
- [10] J. E. Hansen, *Spherical Near-Field Antenna Measurements*. IET, 1988.
- [11] A. D. Yaghjian and S. R. Best, "Impedance, bandwidth, and Q of antennas," in *IEEE Trans. Antennas Propag.*, vol. 53, no. 4, pp. 1298-1324, April 2005.
- [12] A. C. Newell and G. Hindman, "Scattering reduction in spherical near-field measurements," *2008 IEEE Antennas and Propagation Society International Symposium*, San Diego, CA, USA, 2008, pp. 1-4.